

1

Abstract

2

# Measurement of total hadronic differential cross sections in the LArIAT experiment

3

4

Elena Gramellini

5

2018

6

Abstract goes here. Limit 750 words.

7 **Measurement of total hadronic differential**  
8 **cross sections in the LArIAT experiment**

9 A Dissertation  
10 Presented to the Faculty of the Graduate School  
11 of  
12 Yale University  
13 in Candidacy for the Degree of  
14 Doctor of Philosophy

15 by  
16 Elena Gramellini

17 Dissertation Director: Bonnie T. Fleming

18 Date you'll receive your degree



21

*A mia mamma e mio babbo,*

22

*grazie per le radici e grazie per le ali.*

23

*To my mom and dad,*

24

*thank you for the roots and thank you for the wings.*

# Contents

26	<b>Acknowledgements</b>	<b>vi</b>
27	<b>0 Total Hadronic Cross Section Measurement Methodology</b>	<b>1</b>
28	0.1 Event Selection . . . . .	2
29	0.2 Beamline and TPC Handshake: the Wire Chamber to TPC Match . .	5
30	0.3 The Thin Slice Method . . . . .	7
31	0.3.1 Cross Sections on Thin Target . . . . .	7
32	0.3.2 Not-so-Thin Target: Slicing the Argon . . . . .	8
33	0.4 Procedure testing with truth quantities . . . . .	10
34	0.5 Corrections to Data . . . . .	11
35	<b>1 Preparatory Work</b>	<b>13</b>
36	1.1 Construction of a Monte Carlo Simulation for LArIAT . . . . .	14
37	1.1.1 G4Beamline . . . . .	14
38	1.1.2 Data Driven MC . . . . .	14
39	1.2 Tracking Studies . . . . .	14
40	1.2.1 Study of WC to TPC Match . . . . .	14
41	1.3 Energy Calibration and Studies . . . . .	14
42	1.4 Estimate of Energy Loss before the TPC . . . . .	14
43	<b>2 Negative Pion Cross Section Measurement</b>	<b>15</b>

44	2.1	Raw Cross Section . . . . .	15
45	2.2	Background Subtracted Cross Section . . . . .	15
46	2.3	Efficiency Corrected Cross Section . . . . .	15
47	<b>3</b>	<b>Positive Kaon Cross Section Measurement</b>	<b>16</b>
48	3.1	Raw Cross Section . . . . .	16
49	<b>A</b>	<b>Measurement of LArIAT Electric Field</b>	<b>17</b>

# Acknowledgements

*“Dunque io ringrazio tutti quanti.  
Specie la mia mamma che mi ha fatto così funky.”*  
– Articolo 31, Tanqi Funky, 1996 –

*“At last, I thank everyone.  
Especially my mom who made me so funky.”*  
– Articolo 31, Tanqi Funky, 1996 –

A lot of people are awesome, especially you, since you probably agreed to read  
this when it was a draft.

# Chapter 0

## Total Hadronic Cross Section Measurement Methodology

This chapter describes the general procedure employed to measure a total hadronic differential cross section in LArIAT. Albeit with small differences, both the  $(\pi^-, \text{Ar})$  and  $(K^+, \text{Ar})$  total hadronic cross section measurements rely on the same procedure described in details in the following sections. We start by selecting the particle of interest using a combination of beamline detectors and TPC information (Section 0.1). We then perform a handshake between the beamline information and the TPC tracking to assure the selection of the right TPC track (Section 0.2). Finally, we apply the “thin slice” method and measure the “raw” hadronic cross section (Section 0.3). A series of corrections are then evaluated to obtain the “true” cross section (Section 0.5).

At the end of this chapter, we show a sanity check of the methodology against MC truth information (Section 0.4).



## 0.1 Event Selection

The measurement of the  $(\pi^-, \text{Ar})$  and  $(K^+, \text{Ar})$  total hadronic cross section in LArIAT starts by selecting the pool of pion or kaon candidates and measuring their momentum. This is done through the series of selections on beamline and TPC information described in the next sections. The summary of the event selection in data is reported in Table 1.

### Selection of Beamline Events

As shown in equation 5, we leverage the beamline particle identification and momentum measurement before entering the TPC as in input to evaluate the kinetic energy for the hadrons used in the cross sections measurements. Thus, we select the LArIAT data to keep only events whose wire chamber and time of flight information is registered (line 2 in in Table 1). Additionally, we perform a check of the plausibility of the trajectory inside the beamline detectors: given the position of the hits in the four wire chambers, we make sure the particle's trajectory does not cross any impenetrable material such as the collimator and the magnets steel (line 3 in in Table 1).

	Run-II Negative Polarity	Run-II Positive Polarity
Events Reconstructed in Beamline	158396	260810
Events with Plausible Trajectory	147468	240954
Beamline $\pi^-/\mu^-/e^-$ Candidate	138481	N.A.
Beamline $K^+$ Candidate	N.A	2837
Events Surviving Pile Up Filter	108929	2389
Events with WC2TPC Match	41757	1081
Events Surviving Shower Filter	40841	N.A.
Available Events For Cross Section	40841	1081

Table 1: Number of data events for Run-II Negative and Positive polarity

## 89 Particle Identification in the beamline

90 In data, the main tool to establish the identity of the hadron of interest is the LArIAT  
 91 tertiary beamline, in its function of mass spectrometer. We combine the measurement  
 92 of the time of flight,  $TOF$ , and the beamline momentum,  $p_{Beam}$ , to reconstruct the  
 93 invariant mass of the particles in the beamline,  $m_{Beam}$ , as follows

$$m_{Beam} = \frac{p_{Beam}}{c} \sqrt{\left(\frac{TOF * c}{l}\right)^2 - 1}, \quad (1)$$

94 where  $c$  is the speed of light and  $l$  is the length of the particle's trajectory between  
 95 the time of flight paddels.

96 Figure 1 shows the mass distribution for the Run II negative polarity runs on the  
 97 left and positive polarity runs on the right. We perform the classification of events  
 98 into the different samples as follows:

- 99 •  $\pi/\mu/e$ : mass < 350 MeV
- 100 • kaon: 350 MeV < mass < 650 MeV
- 101 • proton: 650 MeV < mass < 3000 MeV.

102 Lines 4 and 5 in in Table 1 show the number of negative  $\pi/\mu/e$  and positive  $K$   
 103 candidates which pass the mass selection for LArIAT Run-II data.

## 104 TPC Selection: Halo mitigation

105 The secondary beam impinging on LArIAT secondary target produces a plethora of  
 106 particles which propagates downstream. The presence of upstream and downstream  
 107 collimators greatly abates the number of particles tracing down the LArIAT tertiary  
 108 beamline. However, it is possible that more than one particle sneaks into the LArTPC  
 109 during its readout time: the TPC readout is triggered by the particle firing the

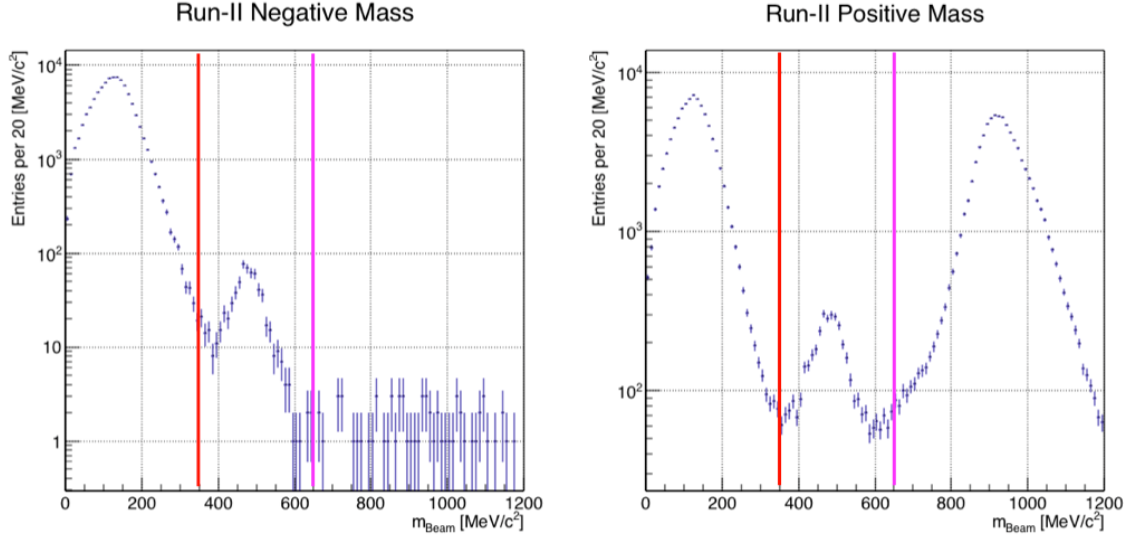


Figure 1: Distribution of the beamline mass as calculated according to equation 1 for the Run-II events reconstructed in the beamline, negative polarity runs on the left and positive polarity runs on the right. The classification of the events into  $\pi^\pm/\mu^\pm/e^\pm$ ,  $K^\pm$ , or (anti)proton is based on these distributions, whose selection cut are represented by the vertical colored lines.

beamline detectors, but particles from the beam halo might be present in the TPC at the same time. We call “pile up” the additional traces in the TPC. We adjusted the primary beam intensity between LArIAT Run I and Run II to reduce the presence of events with high pile up particles in the data sample. For the cross section analyses, we remove events with more than 4 tracks in the first 14 cm upstream portion of the TPC from the sample (line 6 in in Table 1).

### TPC Selection: Shower Removal

In the case of the  $(\pi^-, \text{Ar})$  cross section, the resolution of beamline mass spectrometer is not sufficient to select a beam of pure pions. In fact, muons and electrons survive the selection on the beamline mass. It is important to notice that the composition of the negative polarity beam is mostly pions, as will be discussed in section 1.1.1. Anyhow, we devise a selection on the TPC information to mitigate the presence of

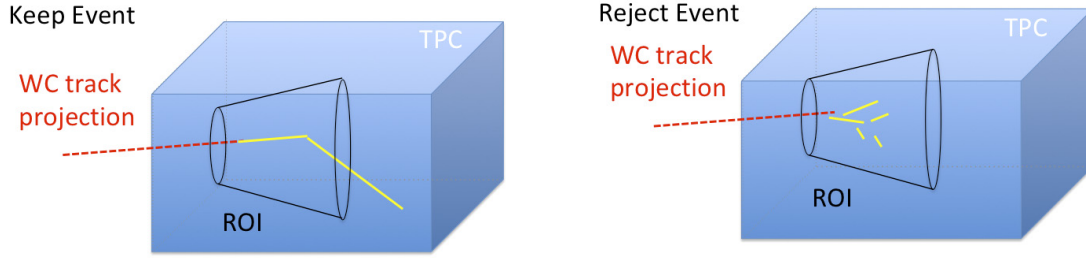


Figure 2: Visual rendering of the shower filter. The ROI is a cut cone, with a small radius of 4 cm, a big radius of 10 cm and an height of 42 cm (corresponding to 3 radiation lengths for electrons in Argon).

122 electrons in the sample used for the pion cross section. The selection relies on the  
 123 different topologies of a pion and an electron event in the argon: while the former  
 124 will trace a track inside the TPC active volume, the latter will tend to “shower”, i.e.  
 125 interact with the medium, producing bremsstrahlung photons which pair convert into  
 126 several short tracks. In order to remove the shower topology, we create a region of  
 127 interest (ROI) around the TPC track corresponding to the beamline particle (more  
 128 details on this in the next section). We look for short tracks contained in the ROI,  
 129 as depicted in figure 4: if more then 5 tracks shorter than 10 cm are in the ROI,  
 130 we reject the event. Line 8 in in Table 1) shows the number of events surviving this  
 131 selection.

## 132 0.2 Beamline and TPC Handshake: the Wire Cham- 133 ber to TPC Match

134 For each event passing the selection on its beamline information, we need to identify  
 135 the track inside the TPC corresponding to the particle which triggered the beamline  
 136 detectors, a procedure we refer to as “WC to TPC match” (WC2TPC for short).  
 137 In general, the TPC tracking algorithm will reconstruct more than one track in the  
 138 event, partially due to the fact that hadrons interact in the chamber and partially

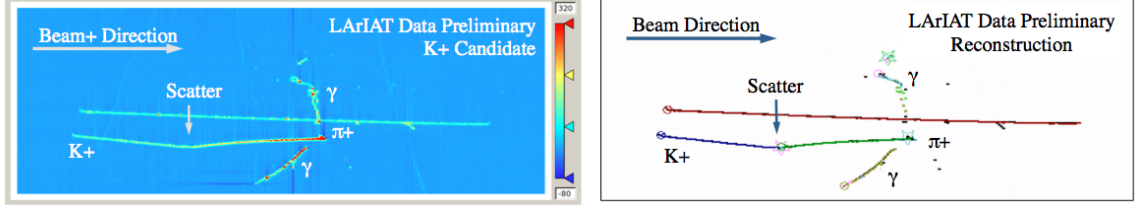


Figure 3: Kaon candidate event: on the right, event display showing raw quantities; on the left, event display showing reconstructed tracks. In the reconstructed event display, different colors represent different track objects. A kink is visible in the kaon ionization, signature of a hadronic interaction: the tracking correctly stops at the kink position and two tracks are formed. An additional pile-up track is so present in the event (top track).

139 because of pile up particles during the triggered TPC readout time, as shown in  
 140 figure 3.

141 We attempt to uniquely match one wire chamber track to one and only one re-  
 142 constructed TPC track. In order to determine if the presence of a match, we apply  
 143 a geometrical selection on the relative the position of the wire chamber and TPC  
 144 tracks. We start by considering only TPC tracks whose first point is in the first 2  
 145 cm upstream portion of the TPC for the match. We project the wire chamber track  
 146 to the TPC front face where we define the coordinates of the projected point as  $x_{FF}$   
 147 and  $y_{FF}$ . For each considered TPC track, we define  $\Delta X$  as the difference between  
 148 the  $x$  position of the most upstream point of the TPC track and  $x_{FF}$ .  $\Delta Y$  is defined  
 149 analogously. We define the radius difference,  $\Delta R$ , as  $\Delta R = \sqrt{\Delta X^2 + \Delta Y^2}$ . We de-  
 150 fine as  $\alpha$  the angle between the incident WC track and the TPC track in the plane  
 151 that contains them. If  $\Delta R < 4$  cm,  $\alpha < 8^\circ$ , a match between WC-track and TPC  
 152 reconstructed track is found. We describe how we determine the value for the radius  
 153 and angular selection in sec 1.2.1. In MC, we mimic the matching between the WC  
 154 and the TPC track by constructing a fake WC track using truth information at wire  
 155 chamber four. We then apply the same WC to TPC matching algorithm as in data.  
 156 We discard events with multiple WC2TPC matches. We use only those TPC tracks  
 157 that are matched to WC tracks in the cross section calculation.

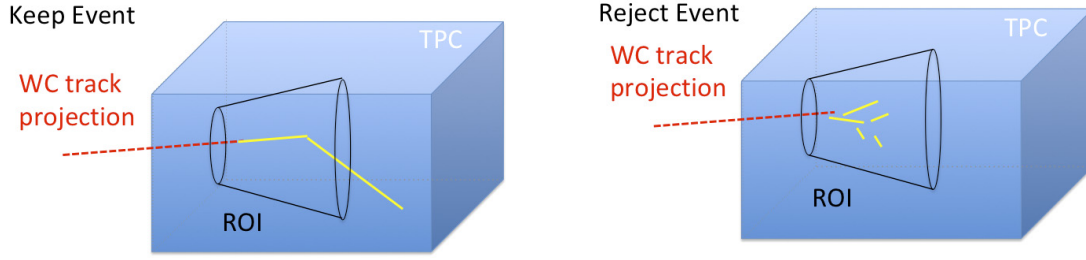


Figure 4: Visual rendering of the wire chamber to TPC match.

## 0.3 The Thin Slice Method

### 0.3.1 Cross Sections on Thin Target

Cross section measurements on a thin target have been the bread and butter of nuclear and particle experimentalists since the Geiger-Marsden experiments [?]. At their core, these types of experiments consist in shooting a beam of particles with a known flux on a thin target and recording the outgoing flux.

In general, the target is not a single particle, but rather a slab of material containing many diffusion centers. The so-called “thin target” approximation assumes that the target centers are uniformly distributed in the material and that the target is thin compared to the interaction length so that no center of interaction sits in front of another. In this approximation, the ratio between the number of particles interacting in the target  $N_{Interacting}$  and number of incident particles  $N_{Incident}$  determines the interaction probability  $P_{Interacting}$ , which is the complementary to one of the survival probability  $P_{Survival}$ . Equation 2

$$P_{Survival} = 1 - P_{Interacting} = 1 - \frac{N_{Interacting}}{N_{Incident}} = e^{-\sigma_{TOT}n\delta X} \quad (2)$$

describes the probability for a particle to survive the thin target. This formula relates the total cross section  $\sigma_{TOT}$ , the density of the target centers  $n$  and the thickness of

the target along the incident hadron direction  $\delta X$ , to the interaction probability<sup>1</sup>. If the target is thin compared to the interaction length of the process considered, we can Taylor expand the exponential function in equation 2 and find a simple proportionality relationship between the number of incident and interacting particles, and the cross section, as shown in equation 3:

$$1 - \frac{N_{Interacting}}{N_{Incident}} = 1 - \sigma_{TOT} n \delta X + O(\delta X^2). \quad (3)$$

Solving for the cross section, we find:

$$\sigma_{TOT} = \frac{1}{n \delta X} \frac{N_{Interacting}}{N_{Incident}}. \quad (4)$$

### 0.3.2 Not-so-Thin Target: Slicing the Argon

The LArIAT TPC, with its 90 cm of length, is not a thin target. However, the fine-grained tracking of the LArIAT LArTPC allows us to treat the argon volume as a sequence of many adjacent thin targets.

As described in Chapter ??, LArIAT wire planes consist of 240 wires each. The wires are oriented at +/- 60° from the vertical direction at 4 mm spacing, while the beam direction is oriented 3 degrees off the  $z$  axis in the  $XZ$  plane. The wires collect signals proportional to the energy loss of the hadron along its path in a  $\delta X = 4 \text{ mm} / \sin(60^\circ) \approx 4.7 \text{ mm}$  slab of liquid argon. Thus, one can think to slice the TPC into many thin targets of  $\delta X = 4.7 \text{ mm}$  thickness along the direction of the incident particle, making a measurement at each wire along the path.

Considering each slice  $j$  a “thin target”, we can apply the cross section calculation from Eq. 4 iteratively, evaluating the kinetic energy of the hadron as it enters each

---

1. The scattering center density in the target,  $n$ , relates to the argon density  $\rho$ , the Avogadro number  $N_A$  and the argon molar mass  $m_A$  as  $n = \frac{\rho N_A}{m_A}$ .

193 slice,  $E_j^{kin}$ . For each WC-to-TPC matched particle, the energy of the hadron entering  
 194 the TPC is known thanks to the momentum and mass determination by the tertiary  
 195 beamline,

$$E_{FrontFace}^{kin} = \sqrt{p_{Beam}^2 - m_{Beam}^2} - m_{Beam} - E_{loss}, \quad (5)$$

196 where  $E_{loss}$  is a correction for the energy loss in the dead material between the  
 197 beamline and the TPC front face. The energy of the hadron at each slab is determined  
 198 by subtracting the energy released by the particle in the previous slabs. For example,  
 199 at the  $j^{th}$  point of a track, the kinetic energy will be

$$E_j^{kin} = E_{FrontFace}^{kin} - \sum_{i < j} \Delta E_i, \quad (6)$$

200 where  $\Delta E_i$  is the energy deposited at each argon slice before the  $j^{th}$  point as measured  
 201 by the calorimetry associated with the tracking.

202 If the particle enters a slice, it contributes to  $N_{Incident}(E^{kin})$  in the energy bin  
 203 corresponding to its kinetic energy in that slice. If it interacts in the slice, it then  
 204 also contributes to  $N_{Interacting}(E^{kin})$  in the appropriate energy bin. The cross section  
 205 as a function of kinetic energy,  $\sigma_{TOT}(E^{kin})$  will then be proportional to the ratio  
 206  $\frac{N_{Interacting}(E^{kin})}{N_{Incident}(E^{kin})}$ .

207 The statistical uncertainty for each energy bin is calculated by error propagation  
 208 from the statistical uncertainty on  $N_{Incident}$  and  $N_{Interacting}$ . Since the number of  
 209 incident hadrons in each energy bin is given by a simple counting, we assume that  
 210  $N_{Incident}$  is distributed as a poissonian with mean and  $\sigma^2$  equal to  $N_{Incident}$  in each  
 211 bin. On the other hand,  $N_{Interacting}$  follows a binomial distribution: a particle in a  
 212 given energy bin might or might not interact. The square of the variance for the  
 213 binomial is given by

$$\sigma^2 = \mathcal{N} P_{Interacting} (1 - P_{Interacting}); \quad (7)$$



214 since the interaction probability  $P_{Interacting}$  is  $\frac{N_{Interacting}}{N_{Incident}}$  and the number of tries  
 215  $\mathcal{N}$  is  $N_{Incident}$ , equation 7 translates into

$$\sigma^2 = N_{Incident} \frac{N_{Interacting}}{N_{Incident}} \left(1 - \frac{N_{Interacting}}{N_{Incident}}\right) = N_{Interacting} \left(1 - \frac{N_{Interacting}}{N_{Incident}}\right). \quad (8)$$

216  $N_{Incident}$  and  $N_{Interacting}$  are not independent. The uncertainty on the cross section  
 217 is thus calculated as

$$\delta\sigma_{tot}(E) = \sigma_{tot}(E) \left( \frac{\delta N_{Interacting}}{N_{Interacting}} + \frac{\delta N_{Incident}}{N_{Incident}} \right) \quad (9)$$

218 where:

$$\delta N_{Incident} = \sqrt{N_{Incident}} \quad (10)$$

$$\delta N_{Interacting} = \sqrt{N_{Interacting} \left(1 - \frac{N_{Interacting}}{N_{Incident}}\right)}. \quad (11)$$

## 219 0.4 Procedure testing with truth quantities

220 The  $\pi^-$ -Ar and  $K^+$ -Ar total hadronic cross section implemented in Geant4 can be  
 221 used as a tool to validate the measurement methodology. We describe here a closure  
 222 test done on Monte Carlo to prove that the methodology of slicing the TPC retrieves  
 223 the underlying cross section distribution implemented in Geant4 within the statistical  
 224 uncertainty.

225 For pions in the considered energy range, the Geant4 inelastic model adopted to  
 226 is “BertiniCascade”, while the elastic model “hElasticLHEP”. For kaons, the Geant4  
 227 inelastic model adopted to is “BertiniCascade”, while the elastic model “hElasticLHEP”.  
 228 cLHEP”.

229 For the validation test, we fire about 390000 pions and 140000 kaons inside the  
 230 LArIAT TPC active volume using the Data Driven Monte Carlo (see section 1.1.2).

231 We apply the thin-sliced method using only true quantities to calculate the hadron  
 232 kinetic energy at each slab in order to decouple reconstruction effects from issues with  
 233 the methodology. For each slab of 4.7 mm length along the path of the hadron, we  
 234 integrate the true energy deposition as given by the Geant4 transportation model.  
 235 Then, we recursively subtracted it from the hadron kinetic energy at the TPC front  
 236 face to evaluate the kinetic energy at each slab until the true interaction point is  
 237 reached. Doing so, we obtain the true interacting and incident distributions for the  
 238 considered hadron and we obtain the true MC cross section as a function of the hadron  
 239 true kinetic energy.

240 Figure 5 shows the total hadronic cross section for argon implemented in Geant4  
 241 10.01.p3 (solid lines) overlaid with the true MC cross section as obtained with the  
 242 sliced TPC method (markers) for pions on the left and kaons on the right; the total  
 243 cross section is shown in green, the elastic cross section in blue and the inelastic  
 244 cross section in red. The nice agreement with the Geant4 distribution and the cross  
 245 section obtained with the sliced TPC method gives us confidence in the validity of  
 246 the methodology.

## 247 **0.5 Corrections to Data**

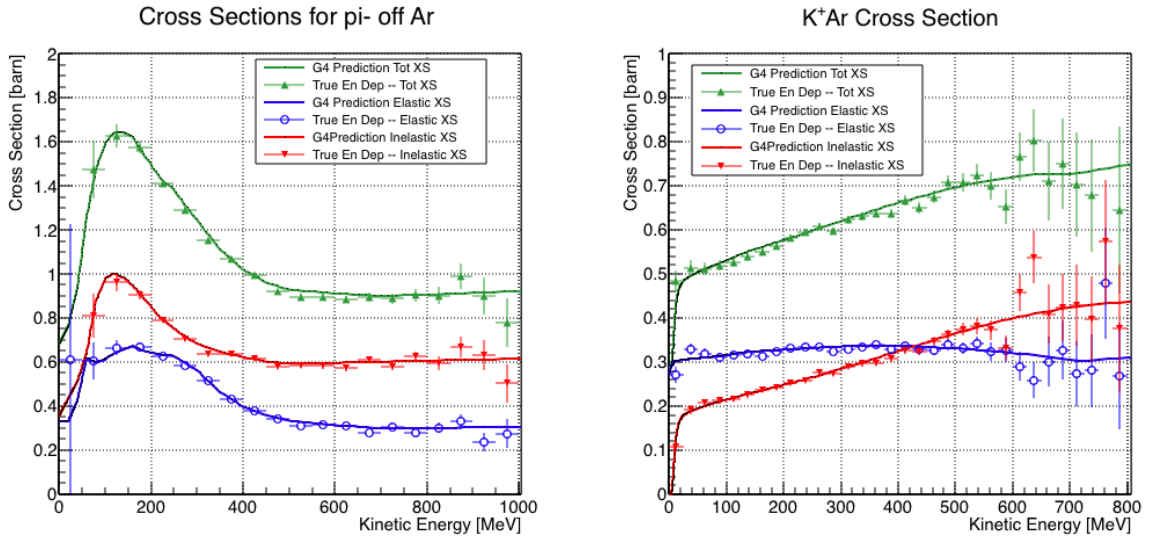


Figure 5: Hadronic cross sections for  $\pi^-$ -Ar (left) and  $K^+$ -Ar (right) implemented in Geant4 10.01.p3 (solid lines) overlaid the true MC cross section as obtained with the sliced TPC method (markers). The total cross section is shown in green, the elastic cross section in blue and the inelastic cross section in red.

# Chapter 1

## Preparatory Work

This chapter describes the preparatory work done on the the data and Monte Carlo samples used for the cross section analyses. This entails:

1. the MC production,
2. the energy calibration of the detector both in data and MC,
3. the optimization of the tracking algorithm for the total cross section analyses.

255 **1.1 Construction of a Monte Carlo Simulation for**  
256 **LArIAT**

257 **1.1.1 G4Beamline**

258 **1.1.2 Data Driven MC**

259 **1.2 Tracking Studies**

260 **1.2.1 Study of WC to TPC Match**

261 **1.3 Energy Calibration and Studies**

262 **1.4 Estimate of Energy Loss before the TPC**

## 263 Chapter 2

# 264 Negative Pion Cross Section 265 Measurement

### 266 2.1 Raw Cross Section

### 267 2.2 Background Subtracted Cross Section

### 268 2.3 Efficiency Corrected Cross Section

## 269 Chapter 3

# 270 Positive Kaon Cross Section

# 271 Measurement

## 272 3.1 Raw Cross Section

## 273 Appendix A

# 274 Measurement of LArIAT Electric 275 Field

276 The electric field of a LArTPC in the drift volume is a fundamental quantity for  
277 the proper functionality of this technology, as it affects almost every reconstructed  
278 quantity such as the position of hits or their collected charge. Given its importance,  
279 we calculate the electric field for LArIAT with a single line diagram from our HV  
280 circuit and we cross check the obtained value with a measurement relying only on  
281 TPC data.

282 Before getting into the details of the measurement procedures, it is important to  
283 explicit the relationship between some quantities in play. The electric field and the  
284 drift velocity ( $v_{drift}$ ) are related as follows

$$v_{drift} = \mu(E_{field}, T)E_{field}, \quad (A.1)$$

285 where  $\mu$  is the electron mobility, which depends on the electric field and on the  
286 temperature (T). The empirical formula for this dependency is described in [?] and  
287 shown in Figure A.1 for several argon temperatures.

288 The relationship between the drift time ( $t_{drift}$ ) and the drift velocity is trivially



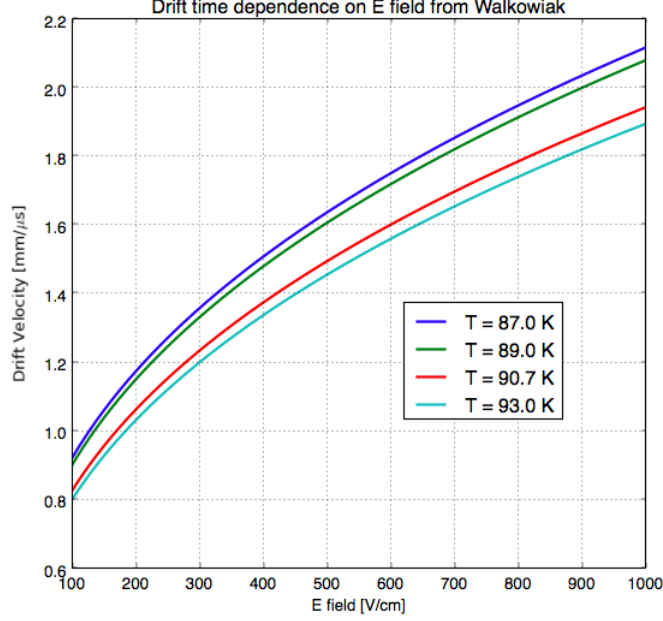


Figure A.1: Drift velocity dependence on electric field for several temperatures. The slope of the line at any one point represents the electron mobility for that given temperature and electric field.

Table A.1: Electric field and drift velocities in LArIAT smaller drift volumes

	Shield-Induction	Induction-Collection
$E_{field}$	700.63 V/cm	892.5 V/cm
$v_{drift}$	1.73 mm/ $\mu$ s	1.90 mm/ $\mu$ s
$t_{drift}$	2.31 $\mu$ s	2.11 $\mu$ s

289 given by

$$t_{drift} = \Delta x / v_{drift}, \quad (\text{A.2})$$

290 where  $\Delta x$  is the distance between the edges of the drift region. Table A.1 reports the  
 291 values of the electric field, drift velocity, and drift times for the smaller drift volumes.

292 With these basic parameters established, we can now move on to calculating the  
 293 electric field in the main drift region (between the cathode and the shield plane).

## Single line diagram method

The electric field strength in the LArIAT main drift volume can be determined knowing the voltage applied to the cathode, the voltage applied at the shield plane, and the distance between them. We assume the distance between the cathode and the shield plane to be 470 mm and any length contraction due to the liquid argon is negligibly small ( $\sim 2$  mm).

The voltage applied to the cathode can be calculated using Ohm's law and the single line diagram shown in Figure A.2. A set of two of filter pots for emergency power dissipation are positioned between the Glassman power supply and the cathode, one at each end of the feeder cable, each with an internal resistance of  $40\text{ M}\Omega$ .

Given the TPC resistor chain, the total TPC impedance is  $6\text{ G}\Omega$ . Since the total resistance on the circuit is driven by the TPC impedance, we expect the resulting current to be

$$I = V_{PS}/R_{tot} = -23.5\text{ kV}/6\text{ G}\Omega \sim 4\text{ }\mu\text{A}, \quad (\text{A.3})$$

which we measure with the Glassman power supply, shown in Figure A.3.

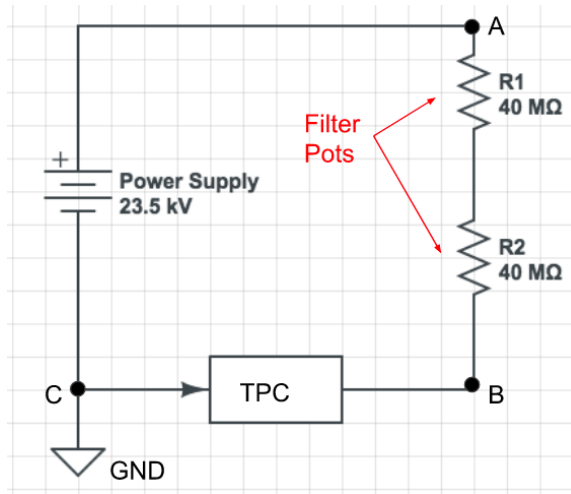


Figure A.2: LArIAT HV simple schematics.

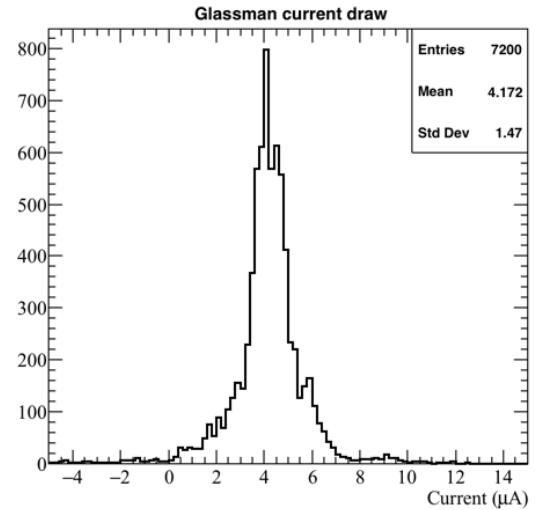


Figure A.3: Current reading from the Glassman between May 25th and May 30th, 2016 (typical Run-II conditions).

308 Using this current, the voltage at the cathode is calculated as

$$V_{BC} = V_{PS} - (I \times R_{eq}) = -23.5 \text{ kV} + (0.00417 \text{ mA} \times 80 \text{ M}\Omega) = -23.17 \text{ kV}, \quad (\text{A.4})$$

309 where  $I$  is the current and  $R_{eq}$  is the equivalent resistor representing the two filter  
310 pots. The electric field is then calculated to be

$$E_{\text{field}} = \frac{V_{BC} - V_{\text{shield}}}{\Delta x} = 486.54 \text{ V/cm}. \quad (\text{A.5})$$

### 311 **E field using cathode-anode piercing tracks**

312 We devise an independent method to measure the drift time (and consequently drift  
313 velocity and electric field) using TPC cathode to anode piercing tracks. We use this  
314 method as a cross check to the single line method. The basic idea is simple:

- 315 0. Select cosmic ray events with only 1 reconstructed track
- 316 1. Reduce the events to the one containing tracks that cross both anode and cath-  
317 ode
- 318 2. Identify the first and last hit of the track
- 319 3. Measure the time difference between these two hits ( $\Delta t$ ).

320 This method works under the assumptions that the time it takes for a cosmic particle  
321 to cross the chamber ( $\sim \text{ns}$ ) is small compared to the charge drift time ( $\sim \text{hundreds}$   
322 of  $\mu\text{s}$ ).

323 We choose cosmic events to allow for a high number of anode to cathode piercing  
324 tracks (ACP tracks), rejecting beam events where the particles travel almost perpen-  
325 dicularly to drift direction. We select events with only one reconstructed track to  
326 maximize the chance of selecting a single crossing muon (no-michel electron). We  
327 utilize ACP tracks because their hits span the full drift length of the TPC, see figure

328 A.4, allowing us to define where the first and last hit of the tracks are located in space  
329 regardless of our assumption of the electric field.

330 One of the main features of this method is that it doesn't rely on the measurement  
331 of the trigger time. Since  $\Delta t$  is the time difference between the first and last hit of a  
332 track and we assume the charge started drifting at the same time for both hits, the  
333 measurement of the absolute beginning of drift time  $t_0$  is unnecessary. We boost the  
334 presence of ACP tracks in the cosmic sample by imposing the following requirements  
335 on tracks:

- 336 • vertical position (Y) of first and last hits within  $\pm 18$  cm from TPC center  
337 (avoid Top-Bottom tracks)
- 338 • horizontal position (Z) of first and last hits within 2 and 86 cm from TPC front  
339 face (avoid through going tracks)
- 340 • track length greater than 48 cm (more likely to be crossing)
- 341 • angle from the drift direction (phi in figure A.5) smaller than 50 deg (more  
342 reliable tracking)
- 343 • angle from the beam direction (theta in figure A.5) greater than 50 deg (more  
344 reliable tracking)

345 Tracks passing all these selection requirements are used for the  $\Delta t$  calculation.

346 For each track passing our selection, we loop through the associated hits to retrieve  
347 the timing information. The analysis is performed separately on hits on the collection  
348 plane and induction plane, but lead to consistent results. As an example of the time  
349 difference, figures A.6 and A.7 represent the difference in time between the last and  
350 first hit of the selected tracks for Run-II Positive Polarity sample on the collection  
351 and induction plane respectively. We fit with a Gaussian to the peak of the  $\Delta t$   
352 distributions to extract the mean drift time and the uncertainty associated with it.

353 The long tail at low  $\Delta t$  represents contamination of non-ACP tracks in the track  
 354 selection. We apply the same procedure to Run-I and Run-II, positive and negative  
 355 polarity alike.

356 To convert  $\Delta t$  recorded for the hits on the induction plane to the drift time we  
 357 employ the formula

$$t_{drift} = \Delta t - t_{S-I} \quad (\text{A.6})$$

358 where  $t_{drift}$  is the time the charge takes to drift in the main volume between the  
 359 cathode and the shield plane and  $t_{S-I}$  is the time it takes for the charge to drift from  
 360 the shield plane to the induction plane. In Table A.1 we calculated the drift velocity  
 361 in the S-I region, thus we can calculate  $t_{S-I}$  as

$$t_{S-I} = \frac{l_{S-I}}{v_{S-I}} = \frac{4mm}{1.73mm/\mu s} \quad (\text{A.7})$$

362 where  $l_{S-I}$  is the distance between the shield and induction plane and  $v_{S-I}$  is the drift  
 363 velocity in the same region. A completely analogous procedure is followed for the hits  
 364 on the collection plane, taking into account the time the charge spent in drifting from  
 365 shield to induction as well as between the induction and collection plane. The value  
 366 for  $\Delta t_{drift}$ , the calculated drift velocity ( $v_{drift}$ ), and corresponding drift electric field  
 367 for the various run periods is given in Table A.2 and are consistent with the electric  
 368 field value calculated with the single line diagram method.

**Delta  $t_{drift}$ , drift  $v$  and E field with ACP tracks**

Data Period	$\Delta t_{Drift} [\mu s]$	Drift velocity $[mm/\mu s]$	E field $[V/cm]$
RunI Positive Polarity Induction	$311.1 \pm 2.4$	$1.51 \pm 0.01$	$486.6 \pm 21$
RunI Positive Polarity Collection	$310.9 \pm 2.6$	$1.51 \pm 0.01$	$487.2 \pm 21$
RunII Positive Polarity Induction	$315.7 \pm 2.8$	$1.49 \pm 0.01$	$467.9 \pm 21$
RunII Positive Polarity Collection	$315.7 \pm 2.7$	$1.49 \pm 0.01$	$467.9 \pm 21$
RunII Negative Polarity Induction	$315.9 \pm 2.6$	$1.49 \pm 0.01$	$467.1 \pm 21$
RunII Negative Polarity Collection	$315.1 \pm 2.8$	$1.49 \pm 0.01$	$470.3 \pm 21$
Average Values	314.1	$1.50 \pm 0.01$	$474.3 \pm 21$

Table A.2:  $\Delta t$  for the different data samples used for the Anode-Cathode Piercing tracks study.

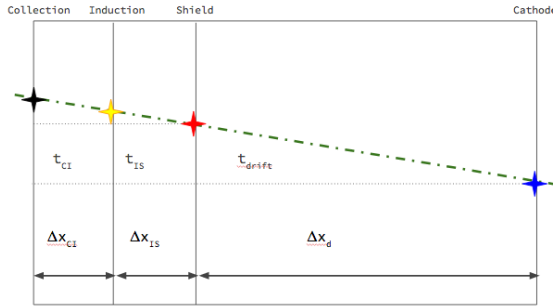


Figure A.4: Pictorial representation of the YX view of the TPC. The distance within the anode planes and between the shield plane and the cathode is purposely out of proportion to illustrate the time difference between hits on collection and induction. An ACP track is shown as an example.

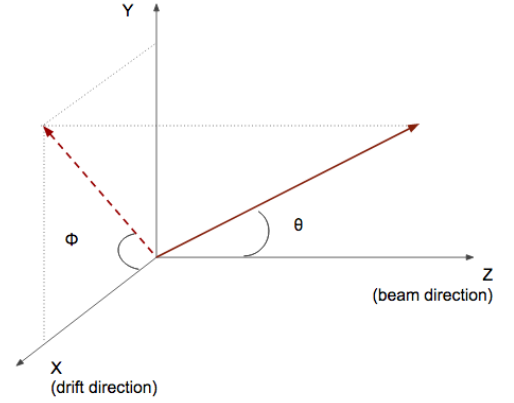


Figure A.5: Angle definition in the context of LArIAT coordinate system.

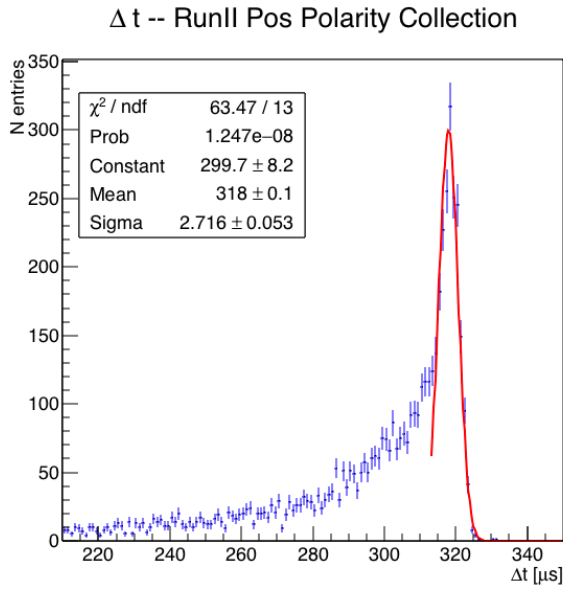


Figure A.6: Collection plane  $\Delta t$  fit for Run II positive polarity ACP data selected tracks.

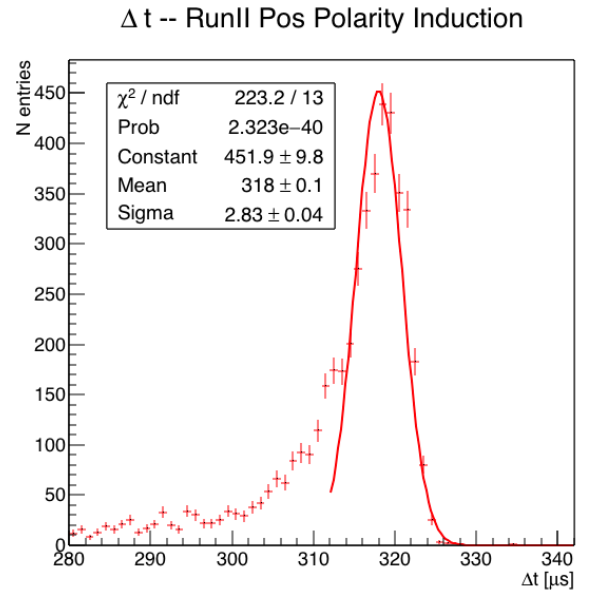


Figure A.7: Induction plane  $\Delta t$  fit for Run II positive polarity ACP data selected tracks.